International Journal of Greenhouse Gas Control 124 (2023) 103855

Contents lists available at ScienceDirect

International Journal of Greenhouse Gas Control

journal homepage: www.elsevier.com/locate/ijggc

Rapid flow diagnostics for prototyping of reservoir concepts and models for subsurface CO_2 storage

D. Petrovskyy [a], C. Jacquemyn [b], S. Geiger [a,*,1], M.D. Jackson [b], G.J. Hampson [b], J.D. Machado Silva [c], S. Judice [c], F. Rahman [c], M. Costa Sousa [c]

[a] Heriot-Watt University, UK
[b] Imperial College London, UK
[c] University of Calgary, Canada

ARTICLE INFO

Keywords:
CO_2 injection
Reservoir modelling
Flow diagnostics
Grid resolution

ABSTRACT

Sketch-based interface and modelling is an approach to reservoir modelling that allows rapid and intuitive creation of 3D reservoir models to test and evaluate geological concepts and hypotheses and thus explore the impact of geological uncertainty on reservoir behaviour. A key advantage of such modelling is the quick creation and quantitative evaluation of reservoir model prototypes. Flow diagnostics capture key aspects of reservoir flow behaviour under simplified physical conditions that enable the rapid solution of the governing equations, and are essential for such quantitative evaluation. In this paper, we demonstrate a novel and highly efficient implementation of a flow diagnostics framework, illustrated with applications to geological storage of CO_2. Our implementation permits 'on-the-fly' estimation of the key reservoir properties that control CO_2 migration and storage during the active injection period when viscous forces dominate. The results substantially improve the efficiency of traditional reservoir modelling and simulation workflows by highlighting key reservoir uncertainties that need to be evaluated in subsequent full-physics reservoir simulations that account for the complex interplay of viscous, gravity, and capillary forces.

The methods are implemented in the open-source Rapid Reservoir Modelling software, which includes a simple to use graphical user interface with no steep learning curve. We present proof-of-concept studies of the new flow diagnostics implementation to investigate the CO_2 storage potential of sketched 3D models of shallow marine sandstone tongues and deep water slope channels.

1. Introduction

Quantifying how the multi-scale geological heterogeneity inherent to many geological formations impacts reservoir behaviour is key to successful CO_2 storage operations, as heterogeneity affects, for example, the available storage volume (Onoja and Shariatipour, 2018), capillary trapping (Harris et al., 2021; Trevisan et al., 2017), CO_2-brine displacement (Reynolds et al., 2018), and possible leakage paths (Armitage et al., 2011). However, geological heterogeneity in CO_2 storage formations is also inherently uncertain and needs to be explored using reservoir models (Alshakri et al., 2023; Jackson et al., 2022). Lack of adequate uncertainty quantification significantly affects the predictability of reservoir models and subsequent reservoir performance forecasts (Arnold et al., 2016; Bentley and Smith, 2008; Christie et al., 2006). Most reservoir modelling workflows are designed to explore and quantify uncertainty around a single geological concept or interpretation scenario (or hypothesis) using stochastic (probabilistic) modelling techniques (Linde et al., 2015; MacDonald et al., 1998). Yet geological model concepts and interpretation scenarios are themselves uncertain and this uncertainty should be explored and its impact on predicted behaviour quantified in a model prototyping stage (Bentley, 2016). Exploring the impact of different geological concepts on CO_2 storage operations interactively and efficiently using subsurface geological models requires rapid and flexible modelling tools that allow users to create, revise and update interpretations and reservoir models quickly, and to explore rapidly how these new interpretations and models change reservoir flow behaviour.

Sketch-based interface and modelling (SBIM) methods have been

* Corresponding author.
E-mail address: s.geiger@tudelft.nl (S. Geiger).
[1] Present address: Delft University of Technology, Netherlands.

https://doi.org/10.1016/j.ijggc.2023.103855
Received 18 August 2022; Received in revised form 9 December 2022; Accepted 2 February 2023
Available online 10 February 2023

applied to quickly build three-dimensional (3D) models from simple 2D sketches as user inputs (Fig. 1). Olsen et al. (2009) and Pereira et al. (2011) demonstrated the application of SBIM to general computer-aided design problems. Natali et al. (2014) created geological models by sketching stratigraphic layers according to their depositional and erosional history. Recently, Jacquemyn et al. (2021b) successfully applied SBIM to build 3D geological models of complex stratigraphy and structure and demonstrated that the SBIM approach is particularly well-suited to explore a range of geological interpretations and concepts, all of which honour available input data, in a few hours rather than days or weeks. Their work documents an efficient reservoir model prototyping approach (Jackson et al., 2015a) for building realistic representations of subsurface heterogeneity, where different geological concepts and scenarios can be sketched in minutes.

The concept of surface-based geological modelling (SBGM) lies at the heart of the SBIM approach (Caumon et al., 2009; Jackson et al., 2014, 2015b; Pyrcz et al., 2005), in which geological heterogeneity is represented using a hierarchy of surfaces (e.g., faults, stratigraphic surfaces, facies boundaries, diagenetic boundaries; Fig. 1). Such representation is geologically intuitive, because the components and processes of model construction are similar to those applied when defining and conceptualising geological relationships in maps, cross-sections and block diagrams. SBIM is used here to create the surfaces produced in SBGM, using specific surface-surface operators to ensure that the interactions between sketched surfaces produce geologically valid models (Jacquemyn et al., 2021b). The surfaces bound geological domains that have similar characteristics at any given scale. Properties such as facies type, rock type, permeability, and porosity, are attributed directly to the domains, which is equivalent to a standard grid-based reservoir modelling approach, but here properties are assigned to geologically meaningful units rather than grid blocks of arbitrary size and shape (Osman et al., 2021). Assigning properties to domains rather than grid blocks is computationally efficient, as the 3D model can be created without reference to an underlying grid. A grid is created only when required for computations.

In this work, we advance the SBIM framework for rapid reservoir prototyping by developing and applying a novel rapid implementation of flow diagnostics (FD) that augments the static representation of geological scenarios with intuitive and fast prototyping of their dynamic behaviour. The FD methods presented in this paper are implemented in a broader toolset referred to as Rapid Reservoir Modelling (RRM) (Jackson et al., 2015a). RRM integrates SBIM functionality with geological operators to construct 3D geologic models (Jackson et al., 2015a), and the 'on-the-fly' flow diagnostics reported here. RRM is available open-source and releases of RRM can be downloaded from https://bitbucket.org/rapidreservoirmodelling/rrm.

FD are controlled numerical experiments that aim to capture key aspects of the reservoir flow behaviour (e.g., breakthrough times, drainage areas, displaced fluid volumes, etc.) under simplified physical conditions (Lie et al., 2015; Møyner et al., 2015; Rasmussen and Lie, 2014) using efficient finite volume discretisations (Aarnes et al., 2007; Eikemo et al., 2009; Natvig and Lie, 2008; Natvig et al., 2007; Noelle et al., 2006) and modern linear solvers (Falgout et al., 2006). FD results can therefore be obtained in a matter of seconds and hence fit well within the rapid SBIM environment, providing agile workflows that allow users to estimate how geological uncertainties impact reservoir volumes and fluid flow behaviours during CO_2 injection. The FD approach presented here focuses on the active injection period when viscous forces dominate fluid flow, especially in the near-wellbore region, not long-term CO_2 migration at the regional or basin scale once the wells have been shut in and gravity and capillary forces dominate. The aim of FD is not to replace traditional 'full-physics' reservoir simulations that capture the complex coupled multi-phase flow processes that occur during CO_2 injection into saline aquifers or depleted hydrocarbon reservoirs (Nicot et al., 2011). Instead, FD help us to explore geological uncertainties and their impact on fluid flow quickly. The results enable us to screen and rank different geological scenarios and models, and to identify the key geological uncertainties that need to be preserved in reservoir models and need to be studied subsequently in more detail using full-physics simulations. RRM allows us to streamlines the design of such CO_2 storage models that explore a plausible range of multi-scale geological uncertainties, and to approximate the dynamic behaviour of

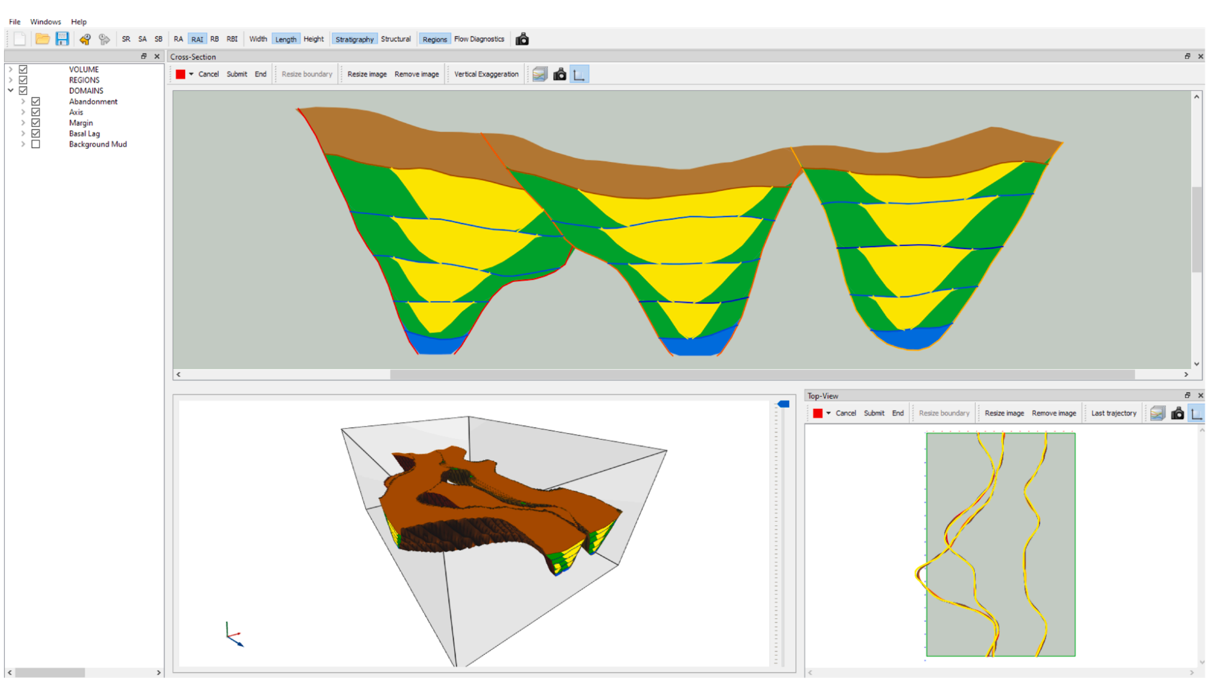

Fig. 1. Overview of the sketch-based interface and modelling framework for reservoir prototyping in RRM (Jacquemyn et al., 2021a). Here, a 3D model of a deep water slope channel complex was created by sketching the 2D architecture of the channels and their associated deposits (upper window) and extruding the 2D sketches along channel thalweg trajectories sketched in plan-view (lower right window) to create a 3D surface-based model (lower left window). Colours denote different facies within the channel-fill deposits.

these reservoir models in an intuitive and time-effective way (Alshakri et al., 2023; Jackson et al., 2022). The resulting model ensemble can be formally compared using clustering techniques based on specific reservoir performance metrics (Scheidt and Caers, 2009; Watson et al., 2021).

In this work, we present a novel implementation of the FD simulation routines and underlying computational framework that facilitate CO_2 storage studies in the RRM context during the active injection phase (Alshakri et al., 2023; Jackson et al., 2022). First, new boundary flow conditions are introduced to enable calculation of the storage potential for injected CO_2. Previous FD works considered wells as boundary conditions and assumed all outer boundaries to be closed (Watson et al., 2021; Zhang et al., 2020). Second, grid resampling 'on-the-fly' is integrated with FD to discretise the surface-based representation of the reservoir geology, which allows grids to be updated while assessing the impact of geological heterogeneity on flow behaviour using FD. Third, FD are incorporated into a highly interactive graphical user interface (GUI) to allow for an intuitive approach to assess the dynamic properties of a given reservoir model. Users can intuitively (i.e., without complicated workflows or menus) populate the reservoir models with the necessary input for dynamic calculations, such as petrophysical properties, well placements or perforation depths, and acquire the dynamic response in near real-time.

The paper is structured as follows. We first describe key elements of the new FD implementation within the RRM toolset that allow for fast dynamic prototyping. We then introduce core aspects of the GUI. Finally, we apply the dynamic FD prototyping approach to two case studies of subsurface CO_2 storage that characterise the impact of geological uncertainty and engineering decisions. The case studies are based on sketched 3D models of a shallow marine shelf and deep water slope channels produced by Jacquemyn et al. (2021a,b).

2. Methods

2.1. Governing equations for flow diagnostics

The fundamental governing equations in FD are based on Darcy's law and assume incompressible single-phase flow, absence of gravity, and mass conservation (Lie et al., 2015; Møyner et al., 2015; Rasmussen and Lie, 2014), which is given by

$$\nabla\cdot\mathbf{v} = q \tag{1}$$

$$\mathbf{v} = \frac{\mathbf{K}}{\mu}\nabla p \tag{2}$$

where $\mathbf{K}$ is the spatially varying permeability tensor, μ is the fluid viscosity, p is the fluid pressure, $\mathbf{v}$ is the fluid velocity, and q is a source or sink term. These approximations are obvious simplifications of the physical processes that occur during CO_2 injection and migration. Hence, as noted above, FD do not replace more time-consuming full-physics simulations but help select appropriate reservoir models for this type of simulation.

The time of flight τ is the central property to FD that characterises flow behaviour. τ is a steady-state quantity that describes the time a virtual and inert particle needs to travel from one point in the reservoir to another based on the flow field. Traditionally, τ has been evaluated using streamlines (Datta-Gupta and King, 2007) but can also be computed directly on the grid of the reservoir model (Shahvali et al., 2012). The definition of τ in Eulerian coordinates is as follows

$$\mathbf{v}\cdot\nabla\tau = \varphi \tag{3}$$

where φ is the spatially varying porosity and the velocity $\mathbf{v}$ is obtained for each grid block from Eq. (2).

Two key metrics are the forward and backward times of flight, τ_f and τ_b, respectively: τ_f denotes the time required for a particle that is released into the reservoir (e.g., at an injection well) to reach a certain point within the reservoir, while τ_b denotes the time required for a particle in the reservoir to reach an outflow boundary (e.g., an offtake well). The sum of τ_f and τ_b yields the residence time $\widehat{\tau}$ in the reservoir, which indicates which areas are contacted quickly by the injected fluid (i.e., CO_2) and which areas are bypassed or only contacted slowly.

To obtain further dynamic properties for FD that approximate the reservoir behaviour such as well allocation factors, drained or swept reservoir regions, influence regions that are affected by the interaction between wells, or the volume of fluid displaced by the injected fluid as a function of time, it is convenient to compute the steady-state concentration c of an inert and virtual tracer for the reservoir (Lie et al., 2015; Møyner et al., 2015; Rasmussen and Lie, 2014; Watson et al., 2021)

$$\mathbf{v}\cdot\nabla c = 0, \ c|_{\text{inflow}} = 1 \tag{4}$$

Shook and Mitchell (2009) demonstrated how other characteristics that approximate the dynamic reservoir behaviour, such as the dynamic Lorenz coefficient, storage efficiency, or breakthrough times, can be calculated from the distribution of τ in the reservoir. Using the storage capacity $\Phi(\tau)$ and flow capacity $\mathrm{F}(\tau)$ given by Møyner et al. (2015)

$$\Phi(\tau) = \int_0^\tau \varphi(r(\widehat{\tau}))\mathrm{d}\widehat{\tau} \tag{5}$$

$$\mathrm{F}(\tau) = \int_0^\tau \frac{\varphi(r(\widehat{\tau}))}{\widehat{\tau}}\mathrm{d}\widehat{\tau} \tag{6}$$

The dynamic Lorenz coefficient L_c can be calculated from $F-\Phi$ curves as

$$L_c = 2\int_0^1 (F(\Phi)-\Phi)d\Phi \tag{7}$$

to quantify the heterogeneity of the flow field where $L_c = 0$ is perfectly homogenous (piston-like) displacement and $L_c = 1$ infinitely heterogeneous displacement. The storage efficiency S_v as a function of pore volumes injected (PVI; also referred to here as dimensionless time t_D) can also be approximated from $F-\Phi$ curves as

$$S_v(t_D) = \Phi + (1-F)t_D \tag{8}$$

$$t_D = \frac{d\Phi}{dF} \tag{9}$$

Watson et al. (2021) showed that these FD properties are useful to screen and rank reservoir model ensembles. Since τ depends on the sketched geology, which governs the spatial distribution of permeability and porosity, and the boundary conditions (e.g., location of wells), any changes to such properties cause an update in the distribution of τ, which can be calculated in a matter of seconds as noted above. Therefore τ and the derived properties provide near real-time, but approximate, feedback on how geological uncertainties could impact CO_2 storage and the migration of CO_2 in the reservoir while CO_2 is being injected. For further details on the numerical calculation of FD and the derivation and application of additional dynamic metrics, such as the Lorenz coefficient, we refer readers to Aarnes et al. (2007); Eikemo et al. (2009); Lie et al. (2015); Møyner et al. (2015); Natvig and Lie (2008); Natvig et al. (2007); Rasmussen and Lie (2014); Shook and Mitchell (2009); Watson et al. (2021).

To assess where in the reservoir CO_2 migration is controlled by viscous forces, we quantify the relative dominance between the gravity and viscous forces through the (transverse) gravity number (Debbabi et al., 2018)

$$N_b = \frac{\Delta\rho g}{\mu}\frac{k_v}{v_h}\frac{L}{H} \tag{10}$$

where $\Delta\rho$ is the density difference between CO_2 and the resident fluid (e.g., brine), g is the standard gravitational acceleration, L and H are the horizontal and vertical length scales respectively, k_v is the vertical permeability, and v_h is the horizontal fluid velocity.

2.2. Surface-based representation to flow diagnostics grid

As outlined above, sketch-based modelling of geology and geological heterogeneity uses a surface-based representation (Jackson et al., 2014, 2015a; Jacquemyn et al., 2021b). Therefore, our models comprise only surfaces (e.g., stratigraphic or structural) that bound geological domains with associated petrophysical properties. However, to perform FD calculation, the models need to be discretised (Natvig and Lie, 2008; Natvig et al., 2007). The surface-based representation of heterogeneity allows for a grid of different resolution to be generated on demand. The grid resolution may be interactively changed to increase (or decrease) the accuracy at which the geological structures are represented as well as the accuracy and speed of the numerical calculations. This flexibility enables users to define an optimal resolution for specific models. Because petrophysical properties are assigned to geological domains, no upscaling or downscaling of properties is required when the grid resolution is changed. In contrast, when using a conventional grid-based approach, reducing the grid resolution to improve calculation efficiency requires upscaling and comes at the cost of less accurate representations of the reservoir geology. In our FD implementation, we discretise the simulation domain using simple Cartesian grids. Such grids are fast to construct, and yield numerically stable monotone flux fields when applying the standard two-point flux approximation and finite volume methods as long as there is k-orthogonality (Natvig et al., 2007; Nordbotten et al., 2007). Whenever grid settings are updated (e.g., location of the origin or resolution), the FD module dynamically matches every cell centre with the domain to which it belongs and assigns the corresponding petrophysical properties. Rapid identification of domains is facilitated by the efficient internal data structures of the surface modelling engine.

2.3. Flow diagnostics computations

The first step is the calculation of the pressure field for the whole model Eq. (1)). As will be discussed below, the pressure field is governed by the constant pressure values in well perforations and model boundaries that interact with the reservoir geology and spatial distribution of petrophysical properties. As noted above, we rely on a structured finite difference grid and a standard two-point flux approximation to discretise the governing equations. The resulting linear system of equations is well-suited for deploying fast and scalable linear solvers such as the algebraic multigrid solvers described by Henson and Yang (2002). The distributions of τ and c are subsequently obtained from the velocity field (Eqs. (3) and ((4)) using a single-point upwind discretisation scheme. The distribution of c is useful to assess the relative contribution of an injection well in multi-well CO_2 injection scenarios. The corresponding matrices are permuted according to the depth-first search approach to rapidly solve the reducible linear system of equations Møyner et al., 2015). Lorenz plots, storage efficiency, breakthrough times and other FD indicators are further extracted from the τ distribution (Eqs. (5) to ((9)). Shahvali et al. (2012) outlined the necessary steps to compute such FD indicators on general grids. If a well is interactively moved to a new location in the model, if the well perforation is changed, or if any other input parameter is changed, the whole computation cycle is immediately re-evaluated to provide information on the reservoir behaviour 'on-the-fly'.

In addition to the essential FD calculations outlined above, we estimate the effective permeabilities for the entire model geometry using flow-based permeability upscaling with no-flow boundary conditions in the direction of flow. This upscaling approach has two key applications. First, it offers the opportunity to obtain effective permeabilities for high-resolution, small-scale geometries which need to be incorporated into larger field-scale models. Second, effective permeabilities for field-scale models are a useful measure for convergence studies of the optimal grid resolution, as will be discussed below.

The basic performance analysis of the FD computations is shown in Fig. 2. The underlying model is a homogeneous cubic grid with two wells in opposite corners. The hardware used is a laptop with Intel® Core™ i5–9300H CPU. When the grid resolution is low, the calculations are almost instantaneous. Even for the grid of 140 × 140 × 140 (almost 3 million cells in total) the total runtime is below 20 s for the pressure solve (~80%) and subsequent FD computation steps (~20%), i.e., topological sorting of the velocity graph and rapid solutions of the τ and c matrices (Møyner et al., 2015). In a multicore processor, effective flow-based permeability calculation is executed in parallel (task-based) and introduces an even smaller performance footprint. Such permeability estimations are useful to assess the effective upscaled behaviour of the larger modelling volume.

Boundary conditions and source terms must be initialised before a numerical flow simulation can take place. In our FD implementation, we allow vertical wells to be created with a single perforated interval (Peaceman, 1983). Additionally, a user may specify inflow/outflow boundary conditions at the vertical boundaries of the model; otherwise, they are non-flowing. Both wells and open boundaries are assigned a fixed pressure. The sketched surface-based reservoir models may not have a flat top and base. For the convenience of flow calculations, the numerical grid is appended with impermeable overburden and underburden to provide no-flow boundaries at the top and bottom of the reservoir model.

2.4. Intuitive user interface

The central component of the FD GUI is an intuitive 3D visualisation and interaction window (Fig. 3). The baseline framework for 3D rendering of our implementation is the Visualisation Toolkit (VTK), an open-source software system for 3D computer graphics, image processing and scientific visualisation (Kitware Inc. 2003; Schroeder et al., 2004). The key advantage of the 3D window implementation is the direct interactions between the user and the FD model. A user may conveniently pick a well in the 3D window using a mouse click or a touchscreen press. Furthermore, the areal location of a well and its perforation interval may be updated swiftly using the drag-and-drop approach. A recorded demonstration of such dynamic interactions is available in Video 1. Therefore, similarly to rapid sketching and surface-based modelling in RRM, the FD module enables visual prototyping of the dynamic flow environment to quickly assess how CO_2 storage (and other injection and withdrawal processes in geological formations) is affected by a given geological scenario. A user may launch the FD module and acquire the corresponding simulation results once the RRM surface-based model is successfully created.

Not all input and output can be entered or visualised in a 3D interface at the desired precision. The 3D window is hence accompanied by a property tree (PT) for precise numerical user input and output. The PT organises settings for input and updates of FD settings (Table 1), such as the name or location of a well, and highlights essential simulation results, such as the breakthrough time for a well. At this stage, a user may specify the grid resolution for flow calculations, as shown in Video 2. The PT properties are grouped by relevant categories for easy navigation.

3. Case studies

Two proof-of-concept case studies are presented, illustrating different aspects of our approach for rapid sketch-based modelling with flow diagnostics for CO_2 storage to (1) quantitatively assess the impact of uncertainty in geological scenarios typically encountered in clastic formations that are targets for CO_2 injection, and (2) screen possible well

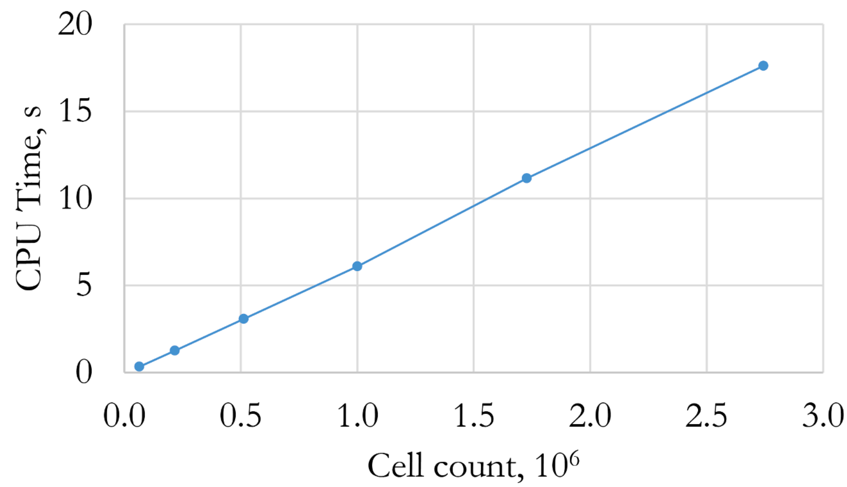

Fig. 2. Evolution of the CPU time for FD computations as a function of grid size on a standard laptop. Grid resolution is uniform in three dimensions.

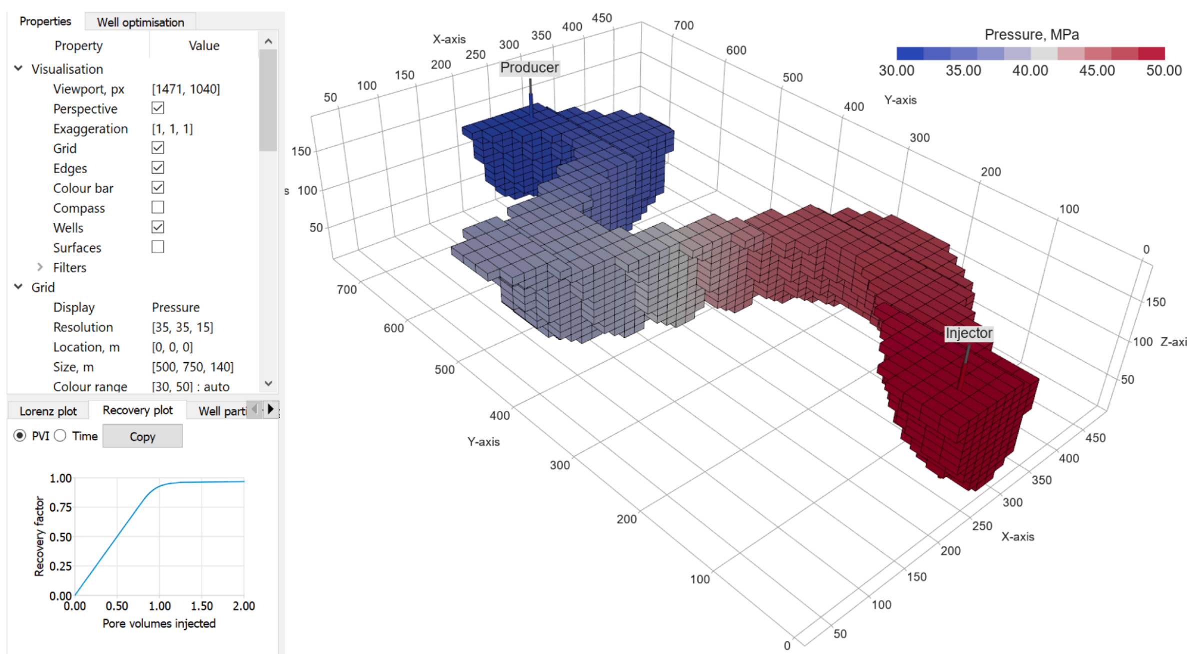

Fig. 3. Screenshot of the FD GUI displaying the 3D pressure field established by the pair of wells located on the opposite sides of a channelised reservoir body.

Table 1
FD output properties.

Output	Purpose
Pore volume, m^3	Basic model characteristics
Total flow rate, m^3/d	
Lorenz coefficient	Indicator of reservoir heterogeneity
Storage at specific PVI	
Storage at specific time	
Breakthrough time for a well, year	
Time of flight distribution, year	
Tracer concentration distribution	
Flow-based effective permeability, mD (x, y, z)	Upscaling of permeability in models and their subregions for representative elementary volume (REV) studies.

locations for CO_2 storage and the impact of grid resolution on model predictions. In both cases, we assume a reservoir depth of approximately 3 km with corresponding standard thermodynamic conditions and CO_2 properties (Heidaryan et al., 2011). We target a CO_2 injection rate of 0.9 Mt/year, which is comparable to the scenario of the Sleipner project (Furre et al., 2016) and adjust the injection pressures accordingly. The summary of the relevant reservoir and fluid properties are provided in Table 2. In all scenarios, we assume a wellbore radius of 10 cm.

Table 2
Reservoir and CO_2 fluid properties used in case studies.

Reservoir property			CO_2 property		
Depth	Pressure	Temperature	Density	Viscosity	Injection rate
3 km	30 MPa	75 °C	767 kg/m^3	$6.76 \cdot 10^{-5}$ Pa·s	3200 m^3/d

3.1. Shallow marine sandstone tongues

Shallow marine sandstone tongues (parasequences) and intercalated shales are considered as storage targets for CO_2 sequestration (Bergmo et al., 2009; Borissova et al., 2013; Calvo and Gvirtzman, 2013). We investigate the impact on flow behaviour and CO_2 storage of geological uncertainty in the stratigraphic architecture of wave- to tide-dominated shallow marine sandstone tongues in the Blackhawk Formation, which are exposed in the Book Cliffs, USA and are analogous to potential CO_2 storage units in the subsurface. Geological models were previously sketched in RRM by Jacquemyn et al. (2021b) to represent different geological scenarios interpreted between five outcrop sections and boreholes (cf. wells). The reservoir models measure approximately 20.5 km by 7.5 km laterally and 60 m in thickness. Five interpretational scenarios are depicted in Fig. 4, showing the sketched surface-based representation (Fig. 4a) and the subsequent discretised representations at a grid resolution of $100 \times 50 \times 100$ (equivalent cell size is 205 $m \times$ 150 $m \times$ 0.6 m) cells for FD analysis (Fig. 4b–f). The underlying facies and their petrophysical properties are listed in Table 3. The differences between the scenarios used are summarised below and discussed in detail in Jacquemyn et al. (2021b).

Scenario SM1 contains high-quality shoreface facies belts (FS, USF, pLSF; Table 3) that are linear in plan-view, mimicking a linear palaeo-shoreline, and have a large dip (palaeo-landward to palaeo-seaward) extent perpendicular to the linear palaeo-shoreline trend (Fig. 4a–b). This scenario was used as a base case from which other scenarios were developed. In scenarios SM2 and SM3, the high-quality shoreface facies belts have a smaller dip extent (SM2; Fig. 4c) or a rugose plan-view trend

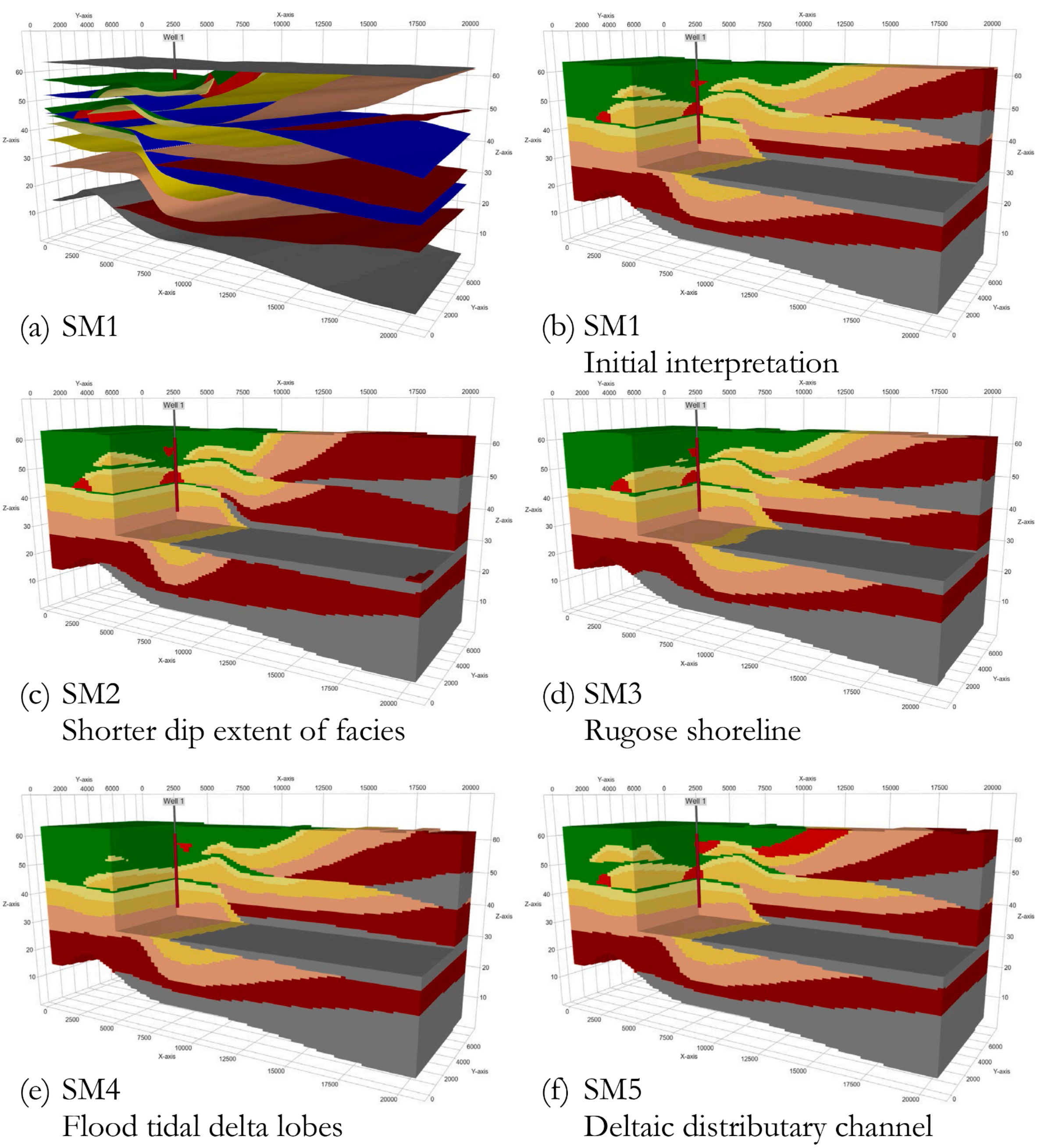

Fig. 4. Surface-based reservoir model of the initial interpretation of the shallow marine strata (a) constructed in RRM by Jacquemyn et al. (2021b). The corresponding models sampled on a grid (b–f) for the different interpretational scenarios illustrate the variation of geological heterogeneity. A single well is present, perforated down to the lowest occurrence of pLSF facies. The legend is provided in Table 3.

Table 3
Facies of the shallow marine strata represented as geological domains in Fig. 4 and their corresponding petrophysical properties.

Facies		Porosity	Permeability	
			Horizontal	Vertical
	Coastal Plain (CP)	3%	3 mD	1 mD
	Foreshore (FS)	23%	1000 mD	500 mD
	Upper Shoreface (USF)	18%	500 mD	50 mD
	Proximal Lower Shoreface (pLSF)	11%	80 mD	5 mD
	Distal Lower Shoreface (dLSF)	6%	5 mD	0.3 mD
	Offshore Transition Zone (OTZ)	0.01%	0.01 mD	0.001 mD
	Channel/Flood Tidal Delta (CH/FTD)	25%	3000 mD	1000 mD

(SM3; Fig. 4d). Flood tidal delta facies (FTD; Table 3) are represented as a continuous, shoreline-parallel belt in four scenarios (SM1, SM2, SM3, SM5), but as discontinuous lobate bodies in scenario SM4 (Fig. 4e). Channel facies (CH; Table 3) are represented as a single linear body that is sub-perpendicular to the palaeo-shoreline in four scenarios (SM1, SM2, SM3, SM4), but as a distributive network that branches down-dip (palaeo-seaward) towards a lobate palaeo-shoreline in scenario SM5 (Fig. 4f). The volumetric facies contributions in each of the five scenarios are summarised in Fig. 5.

A vertical injection well is placed, targeting flood tidal deltas and channelised fluvio-tidal sandbodies in the up-dip (palaeo-landward) part of several vertically stacked sandstone tongues. The well is perforated across the high-quality foreshore and upper shoreface facies (Fig. 4). The top and base boundaries of the model are non-flowing while the four sides are open and assigned fixed pressure values. The injection wellbore pressure is selected independently to match the same injection target flow rate in every scenario. In such a way, we establish a pressure drop primarily in the lateral direction that is representative of the flowing plume configuration when injecting CO_2 into a saline aquifer with low to zero dip and no significant faults. Tables 2 and 4 summarise key reservoir model and fluid properties for the shallow marine case study. The distributions of τ_f and τ_b for scenario SM1 are depicted in Fig. 6. The distribution of τ_f shows preferential flow along high-quality facies and the separation of flow into different branches. Filtered snapshots of τ_f, as shown in Video 3, serve as a qualitative indicator of the flow pattern and regions where CO_2 can be expected to displace the brine more effectively.

To understand where in the reservoir viscous forces dominate CO_2 migration, which can be approximated on a first-order basis using our FD implementation, we plot N_b in Fig. 7. The magnitude of N_b is, in part, determined by the length scale ratio L/H that is generally large (small thickness and large areal extent). In our example, we consider the extent of the CO_2 front as approximated by τ_f of 20 years (Fig. 8) as the

Table 4
Summary of the reservoir model properties for alternative interpretation scenarios shown in Fig. 4.

Interpretation scenario	SM1	SM2	SM3	SM4	SM5
Physical dimensions	20.5 km × 7.5 km × 60 m				
Grid resolution	100 × 50 × 100				
Cell size	205 m × 150 m × 0.6 m				
Pore volume, 10^6 m^3	680	600	661	665	678
Perforation thickness	27 m				
Boundary pressure	30 MPa				
Borehole pressure, MPa	30.215	30.251	30.253	30.445	30.209
Lorenz coefficient	0.766	0.748	0.758	0.765	0.762

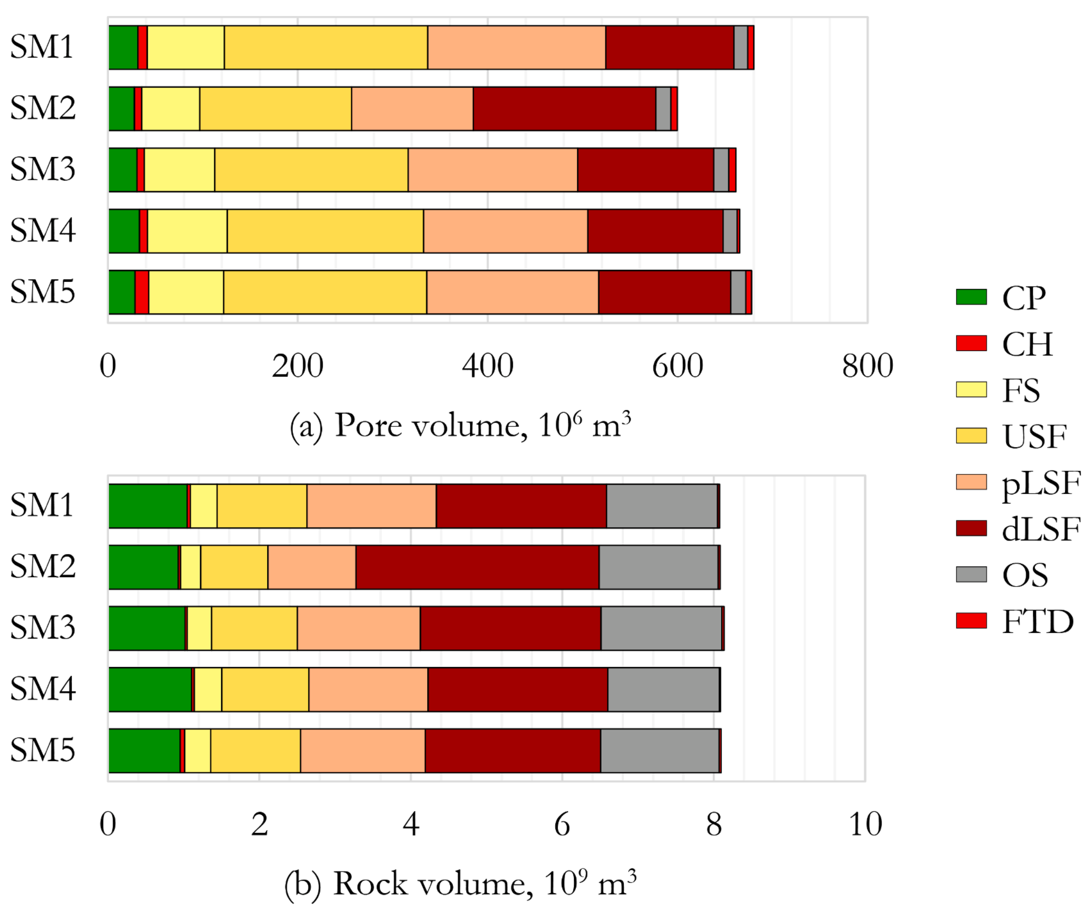

Fig. 5. Facies pore and rock volume distributions for different interpretation scenarios shown in Fig. 4.

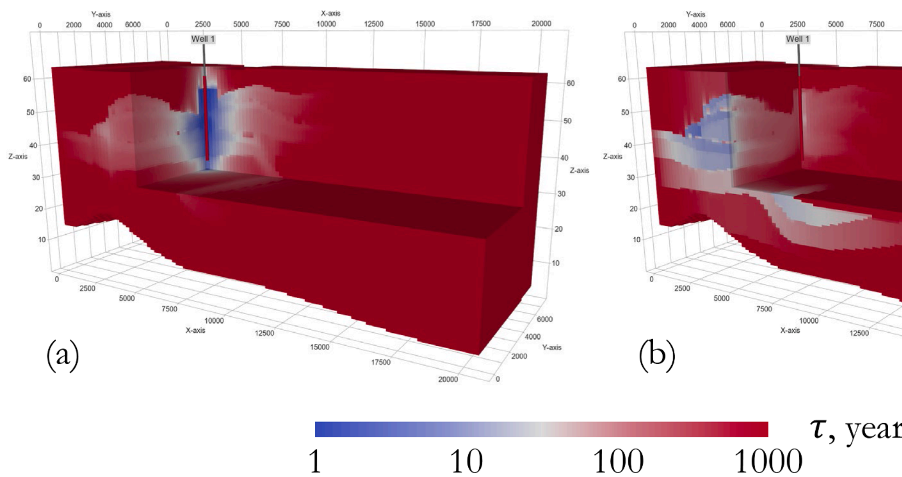

Fig. 6. An illustration of τ_f and τ_b computed for the model SM1 (Fig. 4b), shown in (a) and (b) respectively.

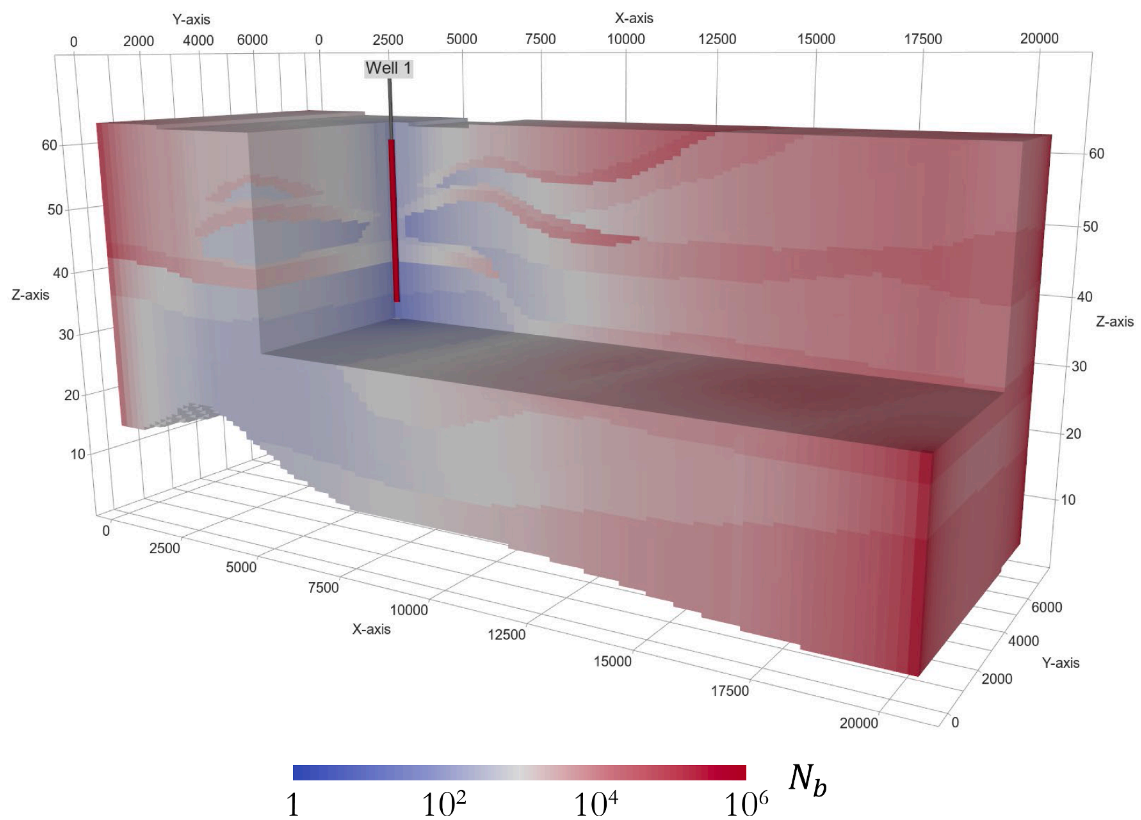

Fig. 7. An illustration of the gravity number N_b computed for model SM1 (Fig. 4b). Lower values correspond to the regions of the reservoir primarily driven by viscous forces.

reference for estimating L/H. Intervals of similar values of N_b illustrate reservoir regions that exhibit similar ratios of viscous-to-gravity forces. More permeable geological facies that are located in the vicinity of the injection wellbore are characterised by viscous-dominated flow while less permeable facies that are located away from the injection well are gravity-dominated.

The permeability heterogeneity associated with the different geological interpretations necessitates different wellbore pressure to sustain the same injection rate (Fig. 4; Table 3). The lowest injection pressure of 30.21 MPa (equivalent pressure differential of 210 kPa) is observed in scenarios SM1 and SM5 with higher proportions of, and good connectivity between, high-quality facies surrounding the injection interval. The highest injection pressure of 30.45 MPa (equivalent pressure differential of 450 kPa) is attributed to SM4, which highlights the impact of continuity of FTD facies, either in a continuous facies belt (SM1, SM2, SM3, SM5; Fig. 4b–d, f) or isolated lobes near the up-dip (palaeo-landward) termination of each sandstone tongue (SM4; Fig. 4e).

To quantitatively assess the influence of uncertainty that is expressed by the different geological interpretations, we compare the extent of the CO_2 fronts after 20 years of injection (approximated as the regions where τ_f is less than 20 years), as shown in Fig. 8. The degree of variation in heterogeneity between different geological scenarios (Fig. 4b–f) results in a spread of the invaded rock volume of around $5 \cdot 10^6$ m^3, as

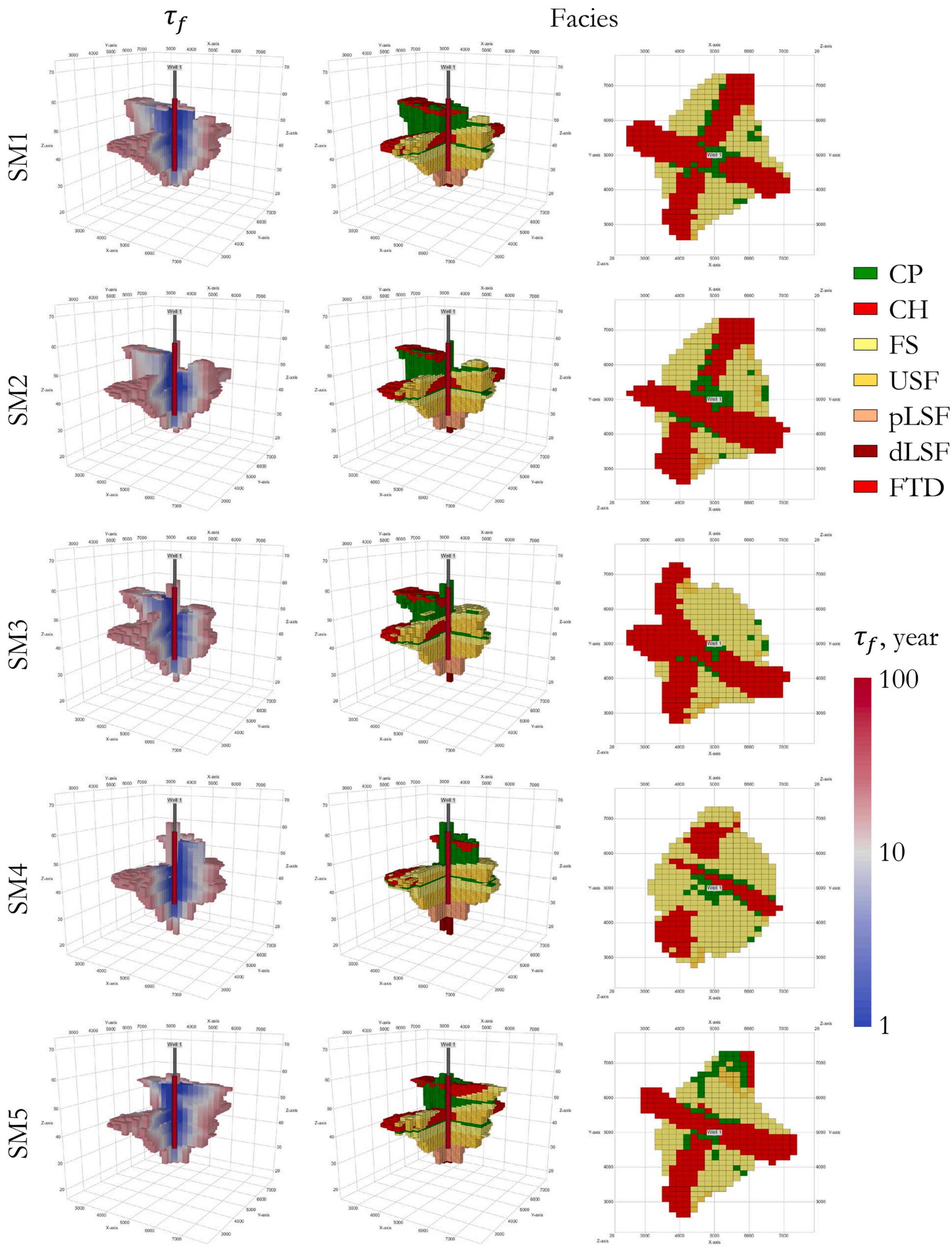

Fig. 8. Filtered distributions of τ_f and invaded facies which approximate the advance of CO_2 after 20 years away from the injection well (note the map-view in the right column). The interpretation scenarios are shown in Fig. 4.

evident from Fig. 9b. The rugose shoreline in SM3 causes a laterally variable and patchy vertical connectivity between successive sandstone tongues (Fig. 4d), resulting in a reduction of invaded rock volume. SM2 has the lowest total pore volume (Fig. 5a) caused by the shorter dip extent of high-quality FS, USF and pLSF facies in each sandstone tongue in this scenario (Fig. 4c), which reduces the vertical connectivity of these facies between successive sandstone tongues and increases the proportion of lower quality dLSF facies. However, in a time frame of 20 years,

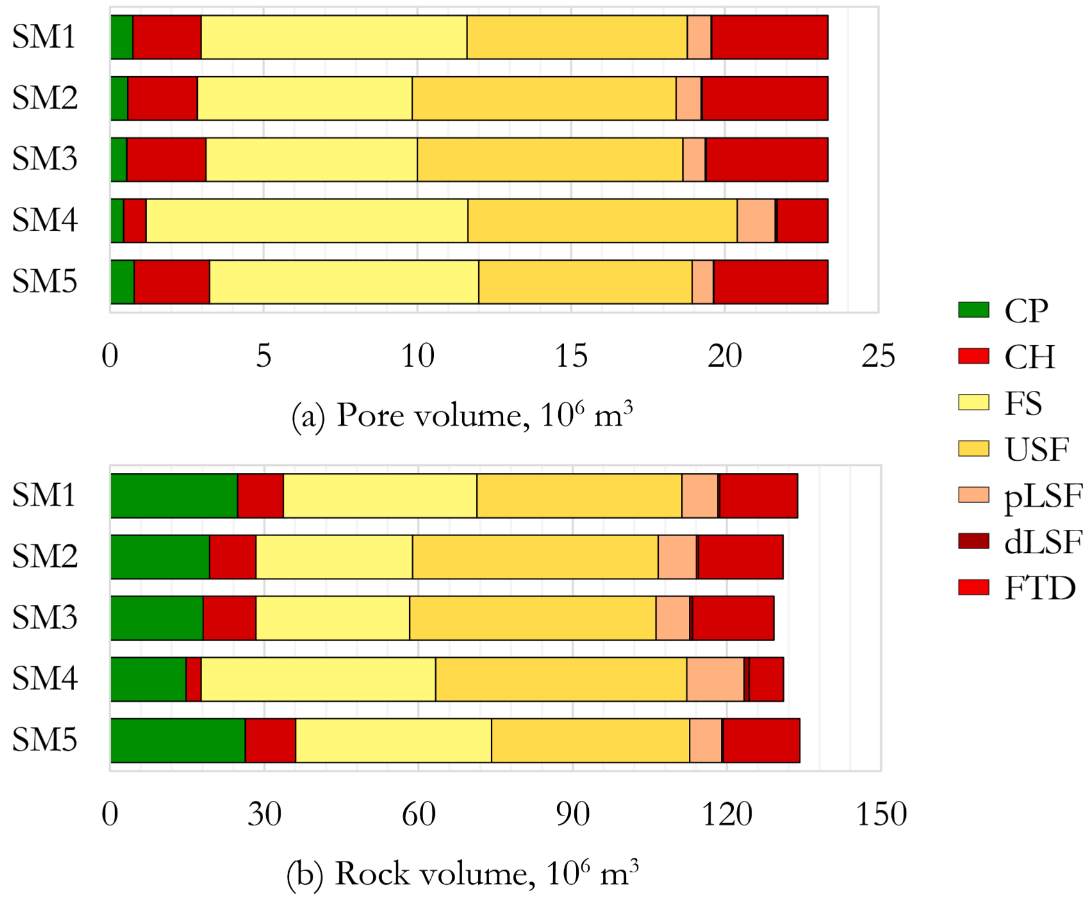

Fig. 9. Pore and rock volume distributions of the facies that are invaded after 20 years of injection (Fig. 8).

the less storable scenario SM2 behaves like the more favourable SM1, as shown in Fig. 8. The similarities in the proportions and connectivities of highest-quality facies (CH, FTD) in scenarios SM1–3 and SM5 (Fig. 4b–d, f) are reflected in similar lateral cross-like shapes of the corresponding invasion fronts (Fig. 8). SM4 invasion is dominated by FS, USF, and pLSF facies that yield a more homogeneous circular lateral displacement front (Figs. 8 and 9).

In this section, we studied the impact of geological heterogeneity and interpretation uncertainty on flow during CO_2 injection in models of shallow marine sandstone parasequences. The FD modelling approach is a powerful tool to integrate and evaluate basic flow properties during the active injection period, such as the pressure-flow rate relationship, the reservoir facies that are most likely invaded by CO_2, or the reservoir regions where viscous and gravity forces prevail. All these insights combined provide a first representative assessment of the CO_2 plume advancement and the key geological uncertainties that control it. While such information can be obtained using conventional reservoir modelling and simulation workflows, RRM and FD allow us to acquire these insights in a very efficient way; typically it takes a day or less to design, build, and explore the full model ensemble.

3.2. *Deep water slope channels*

In this section, we use FD to identify the best placement of a CO_2 injection well and a water extraction well, initially located in opposite corners of a reservoir consisting of channelised sandstones, with water extraction being used to regulate the pressure build up. We also identify the minimum grid resolution that is required to capture the essential features of flow behaviour in this reservoir. The sand-rich channel complex on the Måløy Slope, offshore Norway that forms the basis of the case study was described using seismic data by Jackson et al. (2008). However, there is uncertainty in the detailed stratigraphic architecture of the sandstone at scales below seismic resolution.

Jacquemyn et al. (2021a) constructed multiple interpretations of the channel complex from an original seismic cross-section and RMS amplitude map, with different numbers of channelised elements and different stacking patterns of channel-fill storeys within these elements. The internal architecture of each channelised element (Mayall et al., 2006) is composed of four storeys of channel axis and margin deposits between a basal lag and overlying abandonment mudstones. We use one of the interpreted scenarios (CC1) of Jacquemyn et al. (2021a) to demonstrate the capabilities and impact of ‘on-the-fly’ gridding and interactive exploration of different well patterns. Scenario CC1, shown in Fig. 10 (see also Fig. 1), is characterised by three laterally stacked channelised elements, each of which contains simple vertical stacking of storeys and their constituent channel axis and margin deposits. Petrophysical properties of the corresponding facies are listed in Table 5. Basal lag and channel axis are the most permeable facies in the reservoir model. The model dimensions are 5 km × 7.5 km × 100 m.

Identifying the appropriate grid resolution that captures subsurface heterogeneity and its impact on flow is key for reliable numerical simulation results. Fig. 11 displays the deep water channel complex sampled at increasing grid resolution (the corresponding recording is available as Video 2). As the grid resolution is increased, the original model geometry is captured with increasing accuracy. A key feature of RRM is the possibility to interactively construct a modelling grid of a predefined resolution ‘on-the-fly’ to ensure that geological heterogeneity and connectivity are captured properly. This approach is possible because the underlying surfaces that describe the reservoir architecture are always preserved. Hence the accuracy of subsequent full-physics flow simulations is not restricted to a fixed grid resolution that has been defined at the start of the reservoir modelling process, but the grid

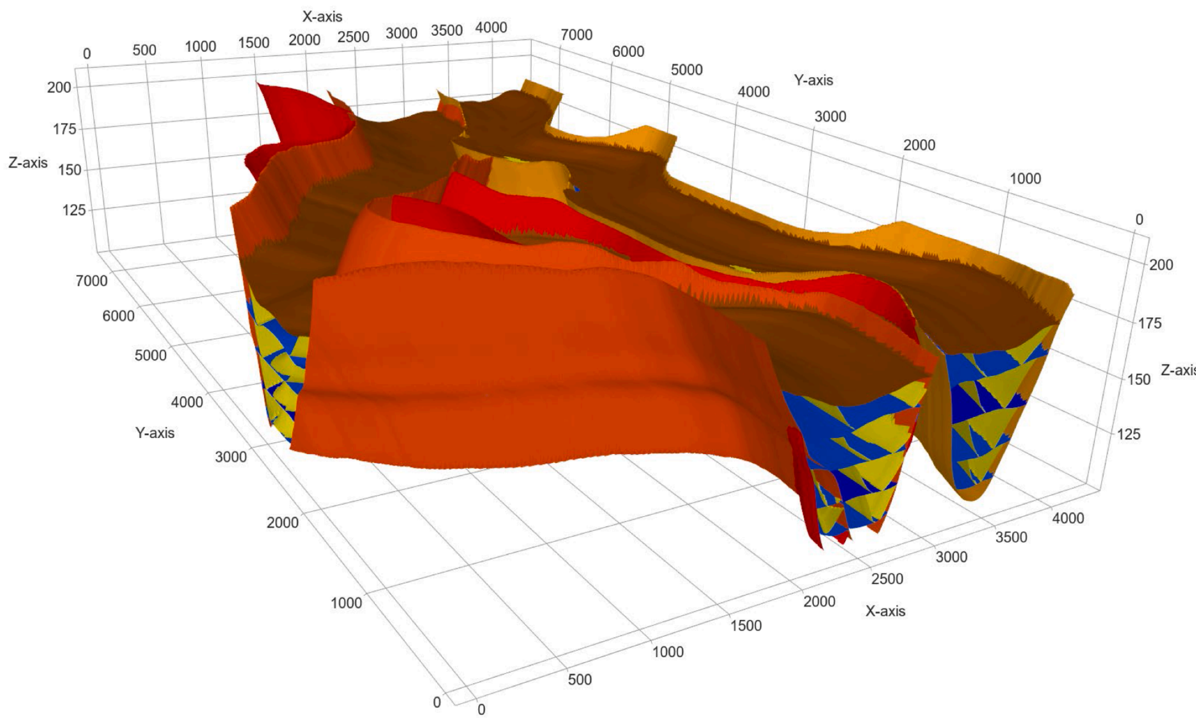

Fig. 10. Surface-based model of the deep water channel complex constructed in RRM by Jacquemyn et al. (2021a).

Table 5
Facies of the deep water slope channel complex represented as geological domains in Fig. 11 and their corresponding petrophysical properties.

Facies		Porosity	Permeability	
			Horizontal	Vertical
(brown)	Abandonment	3%	3 mD	1 mD
(yellow)	Channel Axis	24%	1000 mD	300 mD
(green)	Channel Margin	11%	100 mD	10 mD
(blue)	Basal Lag	26%	3000 mD	2000 mD
(grey)	Background Mud	1%	0.1 mD	0.1 mD

resolution can be adapted to ensure that the fluid flow behaviour is captured accurately. This functionality is further streamlined by providing different FD metrics in RRM that facilitate a-priori grid convergence studies without conducting more time-consuming full-physics simulations.

Fig. 12 shows convergence plots for the effective horizontal (y-direction, subparallel to channel axes) permeability, injection rate, breakthrough time, and Lorenz coefficient for different grid resolutions. The results provide a qualitative and quantitative assessment on how grid resolution impacts the predicted flow behaviour of the same geological model. CO_2-brine displacement is determined by an injector-extraction well pair located on the opposite sides of the model (Fig. 11). Both wells perforate the entire vertical interval of the model. The curves start to converge when the grid resolution exceeds 120 × 120 × 60 (equivalent cell size is 41.7 m × 62.5 m × 1.67 m). A more refined and more representative grid resolution is 180 × 180 × 90 (equivalent cell size is 27.8 m × 41.7 m × 1.1 m). We can hence assume that this particular grid resolution provides the necessary level of detail for a representative FD analysis in this model.

Having identified the minimum necessary grid resolution, we now investigate the placement of the CO_2 injection and water offtake well pair. The offtake well operates at reservoir pressure and the injection well pressure is chosen to meet the target CO_2 injection rate, as provided in Tables 2 and 6. We test the position of the offtake well at four different locations. These configurations include three locations in different channelised elements in the central part of the model and one placed as far as possible from the injector (Fig. 13). All model boundaries are closed to flow. The high-resolution grid of 180 × 180 × 90 (equivalent cell size is 27.8 m × 41.7 m × 1.1 m) is used in this analysis.

Fig. 14 shows the storage efficiency for all positions of the offtake well. As expected, storage efficiency is higher with increasing distance and decreasing connectivity between the injector and extraction wells. Offtake positions 1 and 2 are close and well connected to the injector, and thus have the poorest storage efficiency as injected CO_2 moves quickly between the wells through high-quality channel axis and basal lag facies. Offtake position 3 is located at a similar distance to the injector as offtake positions 1 and 2, but direct connectivity is poor, resulting in the highest storage efficiency. Placing the offtake well as far as possible (position 4) from the injector well does not result in improved storage efficiency in comparison to offtake position 3, because it is not the absolute distance between the wells that ultimately determines the viscous-dominated displacement and subsequent storage efficiency, but the connected flow paths, as shown in Fig. 15. Lorenz coefficients, injection pressure and breakthrough times for the different offtake well placements all suggest similar behaviour (Table 6). This analysis highlights the importance of: (1) the definition of suitable grid resolution using FD, (2) assessment and quantification of interpretational uncertainties using RRM, and (3) the assessment of flow connectivity between wells for storage efficiency, which can be evaluated easily with FD.

4. Discussion

The presented analysis highlights how different interpretational scenarios of subsurface geology could impact the predicted behaviour of subsurface CO_2 sequestration projects. While conventional modelling and simulation workflows can arrive at the same conclusion, they need weeks if not months to execute; here we prototype a geological scenario in a matter of minutes and obtain near real-time feedback on the approximate flow behaviour. Not only do these results help to preserve geological uncertainty when designing detailed reservoir models, they also reduce the turnaround times of conventional modelling and

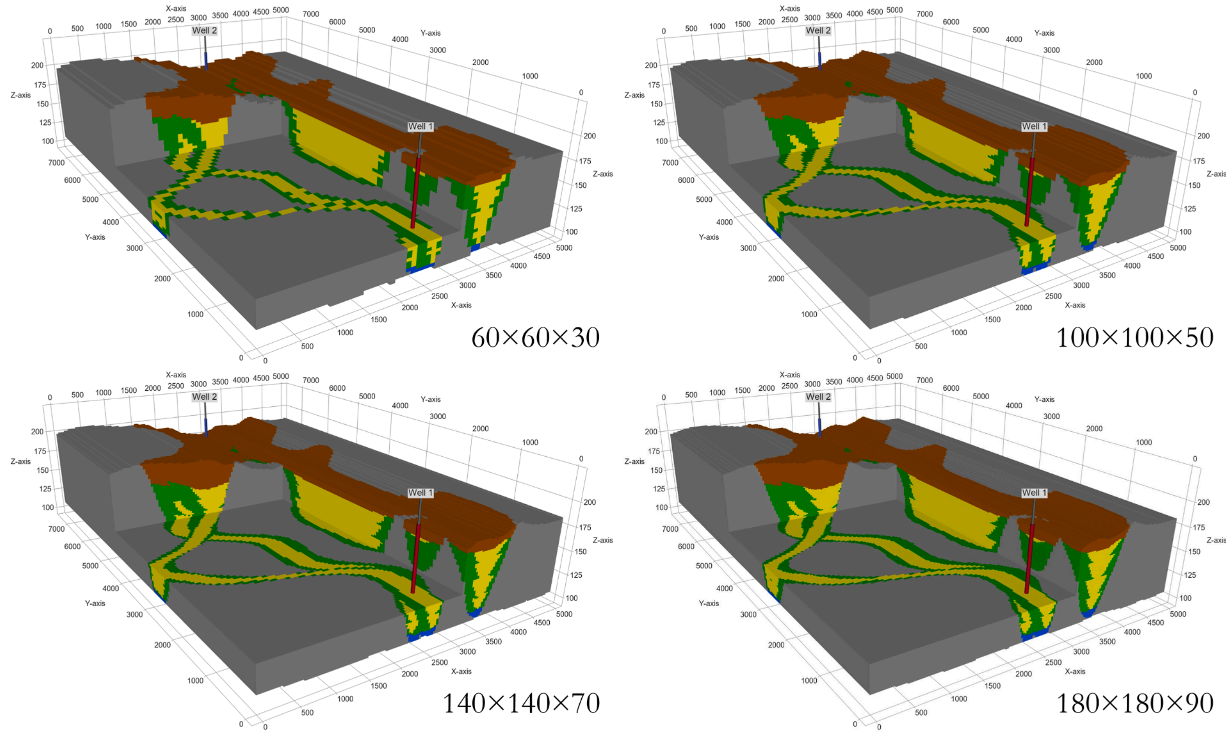

Fig. 11. On-demand grid resampling of a surface-based model representing deep water slope channels at different resolutions. The vertical CO_2 injection (in red) and water offtake (in blue) wells perforate the entire model. A fraction of the grid is hidden to emphasise the distribution of channel axis (yellow) and channel margin (green) facies below the abandonment mudstone (brown) facies.

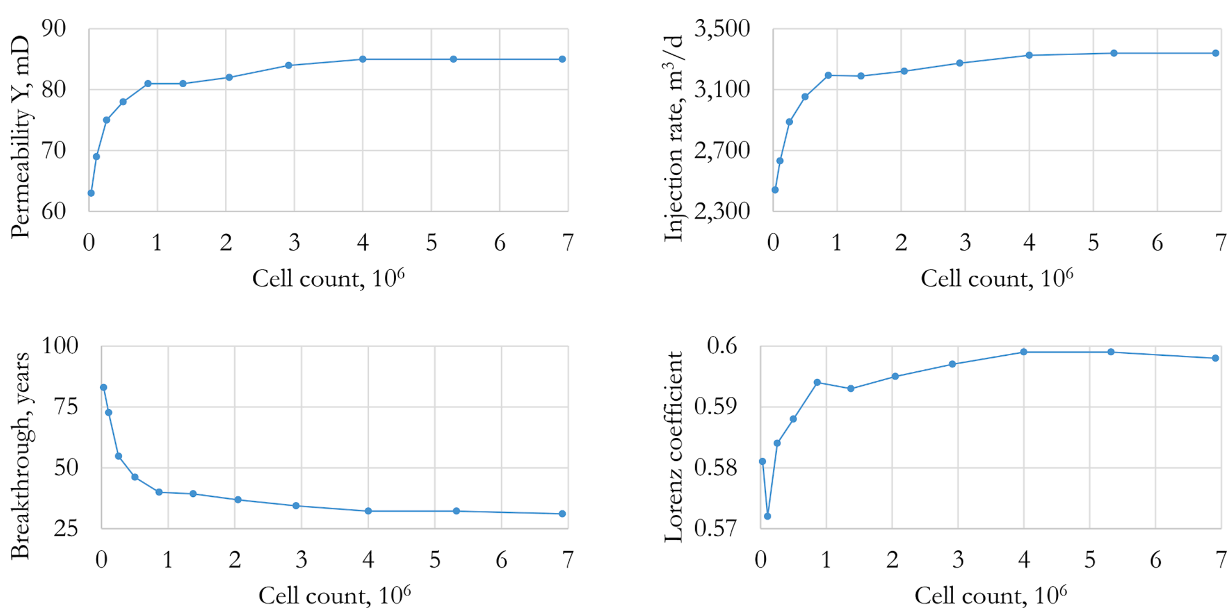

Fig. 12. Convergence plots of the reservoir model properties as functions of grid cell count (resolution). The properties begin to stabilise when the cell count approaches 10^6 (equivalent grid resolution 120 × 120 × 60). A grid of $3{\cdot}10^6$ cells (equivalent grid resolution 180 × 180 × 90) has a higher level of convergence.

simulation workflows, allowing users to direct valuable time in reservoir modelling and simulation where it matters most. 'On-the-fly' resampling and gridding of a surface-based model allowed us to test multiple grid resolutions quickly without any prior upscaling or downscaling, using the FD results to investigate how storage efficiencies and modelling accuracy vary. Such an analysis is not possible in conventional reservoir modelling workflows as the grid resolution becomes fixed early during model construction, and any later changes to the grid cannot add further geological details without resetting the entire geological modelling workflow. Furthermore, results from such prototyping exercises can be used to decide which additional data could be collected to reduce uncertainty (e.g., to investigate the connectivity of FTD facies and the dip extent of FS and USF facies in the first case study). The significant improvements in reservoir prototyping introduced in this paper are summarised below:

1. Quick and easy to use. The RRM framework, together with the FD functionality, provides a user-friendly graphical interface to

Table 6
Summary of the reservoir model properties for different well placement patterns shown in Fig. 13.

Offtake well	Pos 1	Pos 2	Pos 3	Pos 4
Physical dimensions	5 km × 7.5 km × 100 m			
Grid resolution	180 × 180 × 90			
Cell size	27.8 m × 41.7 m × 1.1 m			
Pore volume	$156{\cdot}10^6$ m^3			
Perforation thickness	100 m			
Offtake pressure	30 MPa			
Injection pressure, MPa	30.583	30.361	31.529	30.888
Breakthrough time, years	18.5	6.8	64.6	35.2
Stored at breakthrough, Mt	16.65	6.12	58.14	31.68
Lorenz coefficient	0.828	0.885	0.512	0.597

construct realistic reservoir models simply by sketching on a touch-sensitive screen. Usually, several hours of training are sufficient to learn key prototyping functionalities.

2. Testing geological uncertainty. The ease of creating alternative interpretation scenarios and the efficient implementation of modelling and rapid flow simulations facilitate more comprehensive uncertainty analysis of geological heterogeneity.
3. Grid convergence studies. Interactive sampling of the surface-based reservoir model into simulation grids of different resolution is fast and consistent. The analysis of indicators, such as the total flow rate or breakthrough time, for different grid resolutions enables convenient workflows for grid convergence studies.
4. Well placement optimisation. Convenience and speed of altering well configuration and placement facilities rapid prototyping of alternative injection scenarios to maximise the efficiency.

We reiterate that reservoir prototyping with the ‘on-the-fly’ feedback on dynamic behaviour presented here does not replace traditional reservoir modelling and simulation workflows and should only be applied during the active injection phase when viscous forces dominate. We hence analyse the (transverse) gravity number to identify the regions of the reservoir that are dominated by viscous and gravity forces. The RRM approach with integrated FD complements other effective CO_2 storage modelling techniques such as vertically-integrated equilibrium methods (e.g., Lie et al., 2016; Bandilla et al., 2019) that enable the fast assessment of regional-scale CO_2 migration.

As discussed above, FD is based on simplified reservoir flow processes which are not representative of the complex multi-phase flow physics encountered when CO_2 is injected into saline aquifers or depleted hydrocarbon reservoirs. While more complex physics could be added; for example, using a diffusive time-of-flight to approximate the transient pressure build-up when injecting a compressible fluid (Zhang et al., 2016, 2020) or vertically-integrated equilibrium models to assess regional- and basin-scale CO_2 migration (Lie et al., 2016; Bandilla et al., 2019), the principal idea of reservoir prototyping is to explore a much wider range of geological scenarios and uncertainties, to compare, contrast, and rank the resulting reservoir models, and to select a few reservoir models that display different flow behaviours to preserve the full range of uncertainties for further detailed reservoir modelling and full-physics simulation studies. Methods for robustly comparing, clustering, and ranking reservoir models are well established (Scheidt and Caers, 2009). Hence, our approach to reservoir prototyping allows us to significantly accelerate state-of-the-art uncertainty quantification and robust optimisation workflows for CO_2 storage (Agada et al., 2017).

In future releases we plan to provide functionality to set target injection rates, in addition to fixed pressure. We will facilitate specification of fault transmissibility for more representative flow modelling across faults. Finally, deviated and horizontal wells will become available to complement simple vertical well configurations.

5. Conclusions

In this paper we introduce a novel flow diagnostics functionality within the open-source Rapid Reservoir Modelling environment. The distinct characteristic of our implementation is the ease of use and efficiency of the numerical calculations. The surface-based reservoir models created using RRM’s sketch-based interface and modelling tools can be conveniently and quickly sampled into grids of arbitrary resolution with the desired level of detail. The graphical user interface

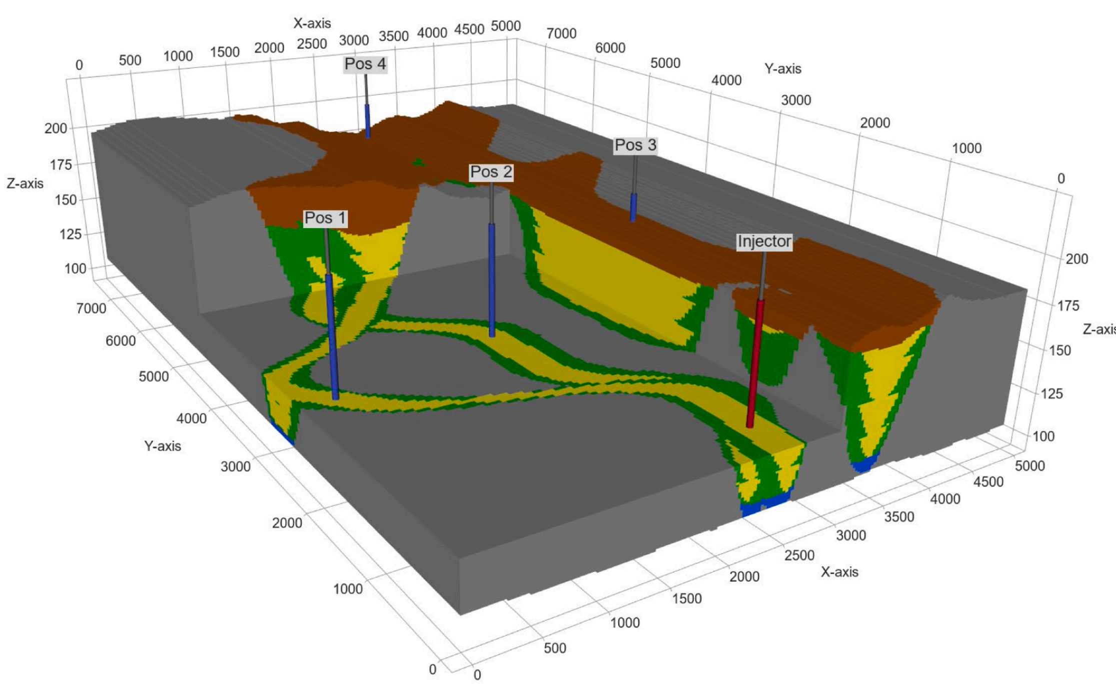

Fig. 13. Different positions considered for the brine offtake well. Position 1 and position 2 are directly connected to the injector via the channel axis (yellow) facies in a shared channelised element, whereas position 3 is in a different channelised element to those penetrated by the injector. Position 4 is located on the opposite side of the model.

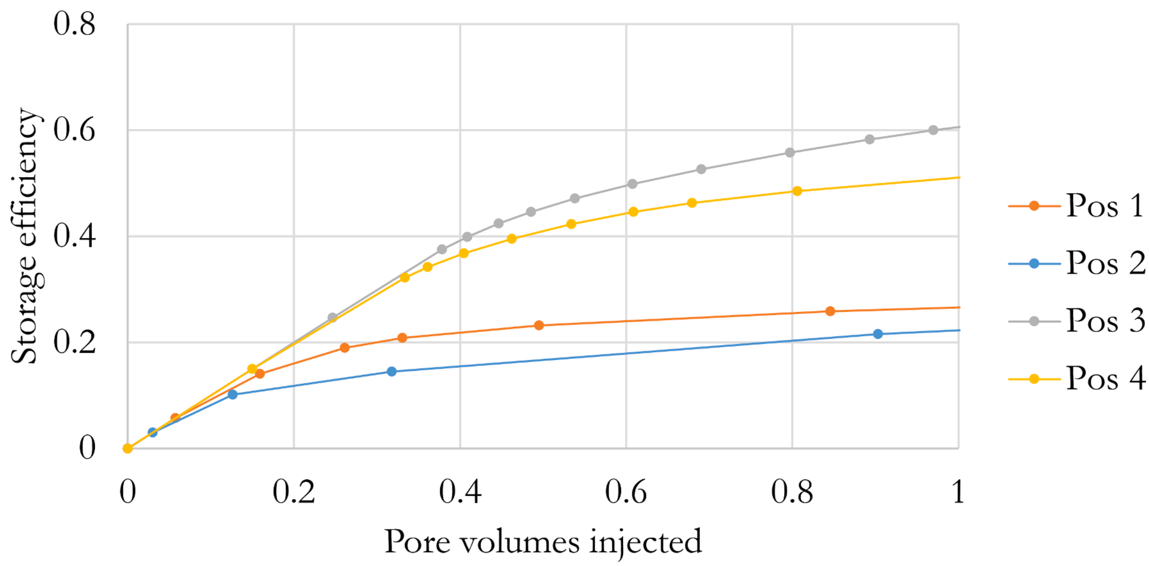

Fig. 14. Storage efficiency curves as a function of pore volumes injected. Well placements of the extraction well are depicted in Fig. 13.

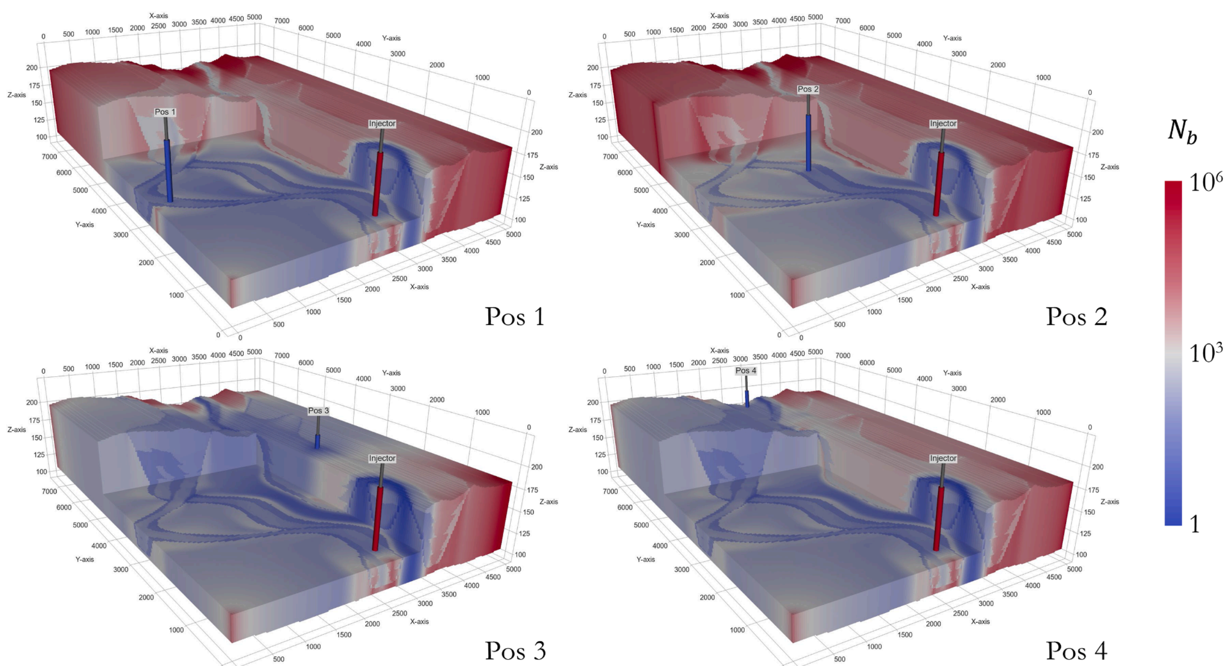

Fig. 15. An illustration of N_b computed for different positions of the offtake well (Fig. 13). Offtake positions 1 and 2 that are directly connected to the injector show that only a fraction of the reservoir is dominated by viscous forces (lower value of N_b). Although similarly positioned, offtake position 3 is not directly connected to the injector through the high permeability channel axis facies and hence displays the highest amount of viscous-dominated flow. Position 4 exhibits intermediate behaviour compared to offtake positions 1, 2 and 3 with respect to the reservoir regions that are dominated by viscous forces.

facilitates intuitive and interactive configuration of vertical wells and the corresponding perforation intervals. Modifications to the input parameters, such as the permeability distribution or the well placement pattern, trigger 'on-the-fly' calculations of the flow diagnostics properties, e.g., the time of flight field and the Lorenz curve. We applied the underlying rapid reservoir modelling tools to study the CO_2 storage potential in models of a shallow marine shelf and deep water slope channel complex.

CRediT authorship contribution statement

D. Petrovskyy: Conceptualization, Methodology, Investigation, Data curation, Software, Writing – original draft, Writing – review & editing. **C. Jacquemyn:** Conceptualization, Data curation, Software, Writing – review & editing. **S. Geiger:** Conceptualization, Methodology, Funding acquisition, Supervision, Writing – original draft, Writing – review & editing. **M.D. Jackson:** Conceptualization, Funding acquisition, Writing – review & editing. **G.J. Hampson:** Conceptualization, Data curation, Funding acquisition, Writing – review & editing. **J.D. Machado Silva:** Software, Writing – review & editing. **S. Judice:** Software, Writing – review & editing. **F. Rahman:** Software, Writing – review & editing. **M. Costa Sousa:** Funding acquisition, Writing – review & editing.

Declaration of Competing Interest

The authors declare the following financial interests/personal relationships which may be considered as potential competing interests:

Sebastian Geiger reports financial support was provided by ExxonMobil Research and Engineering Company Annandale. Sebastian Geiger reports financial support was provided by Petrobras. Sebastian Geiger reports financial support was provided by Petronas Carigali Sdn Bhd. Sebastian Geiger reports financial support was provided by Shell. Sebastian Geiger reports financial support was provided by Equinor ASA. Sebastian Geiger reports financial support was provided by IBM. Sebastian Geiger reports financial support was provided by Energi Simulation.

Data availability

Numerical models that are generated and analysed in this study and relevant screen recordings are available at https://doi.org/10.6084/m9.figshare.c.6038195. Rapid Reservoir Modelling prototype software and source code are available at https://bitbucket.org/rapidreservoirmodelling/rrm.

Acknowledgements

We thank the members of Phase 1 of the Rapid Reservoir Modelling Consortium (Equinor, ExxonMobil Upstream Research Company, Petrobras, Shell, and IBM Research Brazil/IBM Centre for Advanced Studies (CAS) Alberta, Canada) and Phase 2 of the Rapid Reservoir Modelling Consortium (Equinor, ExxonMobil Upstream Research Company, Petrobras, Petronas, and Shell) for funding this work and granting permission to publish this paper. SG acknowledges partial funding for his Chair from Energi Simulation.

References

Aarnes, J.E., Hauge, V.L., Efendiev, Y., 2007. Coarsening of three-dimensional structured and unstructured grids for subsurface flow. Adv. Water Resour. 30, 2177–2193.

Agada, S., Geiger, S., Elsheikh, A., Oladyshkin, S., 2017. Data-driven surrogates for rapid simulation and optimization of WAG injection in fractured carbonate reservoirs. Petrol. Geosci. 23, 270–283.

Alshakri, J., Hampson Gary, J., Jacquemyn, C., Jackson Matthew, D., Petrovskyy, D., Geiger, S., Silva Julio, D.M., Judice, S., Rahman, F., Costa Sousa, M., 2023. A Screening Assessment of the Impact of Sedimentological Heterogeneity On CO2 Migration and Stratigraphic-Baffling Potential: Sherwood and Bunter Sandstones, 528. Geological Society, London, Special Publications, UK. SP528-2022-2034.

Armitage, P.J., Faulkner, D.R., Worden, R.H., Aplin, A.C., Butcher, A.R., Iliffe, J., 2011. Experimental measurement of, and controls on, permeability and permeability anisotropy of caprocks from the CO2 storage project at the Krechba Field, Algeria. J. Geophys. Res.-Sol. Ea 116, 18.

Arnold, D., Demyanov, V., Christie, M., Bakay, A., Gopa, K., 2016. Optimisation of decision making under uncertainty throughout field lifetime: a fractured reservoir example. Comput. Geosci. 95, 123–139.

Bandilla, K., Guo, B., Celia, M.A., 2019. A guideline for appropriate application of vertically-integrated modeling approaches for geologic carbon storage modeling. Int. J. Greenhouse Gas Control 91, 102808.

Bentley, M., 2016. Modelling for comfort? Petrol. Geosci. 22, 3–10.

Bentley, M., Smith, S., 2008. Scenario-based reservoir modelling: the need for more determinism and less anchoring. In: Robinson, A., Griffiths, P., Price, S., Hegre, J., Muggeridge, A. (Eds.), Future of Geological Modelling in Hydrocarbon Development. Geological Soc Publishing House, Bath, pp. 145–159.

Bergmo, P.S., Lindeberg, E., Riis, F., Johansen, W.T., 2009. Exploring geological storage sites for CO2 from Norwegian gas power plants: Johansen formation. Energy Procedia 1, 2945–2952.

Borissova, I., Kennard, J., Lech, M., Wang, L., Johnston, S., Lewis, C., Southby, C., 2013. Integrated approach to CO2 storage assessment in the offshore South Perth Basin, Australia. Energy Procedia 37, 4872–4878.

Calvo, R., Gvirtzman, Z., 2013. Assessment of CO2 storage capacity in southern Israel. Int. J. Greenhouse Gas Control 14, 25–38.

Caumon, G., Collon-Drouaillet, P., Le Carlier de Veslud, C., Viseur, S., Sausse, J., 2009. Surface-based 3D modeling of geological structures. Math. Geosci. 41, 927–945.

Christie, M., Demyanov, V., Erbas, D., 2006. Uncertainty quantification for porous media flows. J. Comput. Phys. 217, 143–158.

Datta-Gupta, A., King, M., 2007. Streamline Simulation: Theory and Practice. Society of Petroleum Engineers.

Debbabi, Y., Jackson, M.D., Hampson, G.J., Salinas, P., 2018. Impact of the buoyancy-viscous force balance on two-phase flow in layered porous media. Transp. Porous Media 124, 263–287.

Eikemo, B., Lie, K.-A., Eigestad, G.T., Dahle, H.K., 2009. Discontinuous Galerkin methods for advective transport in single-continuum models of fractured media. Adv. Water Resour. 32, 493–506.

Falgout, R.D., Jones, J.E., Yang, U.M., 2006. The Design and Implementation of hypre, a Library of Parallel High Performance Preconditioners. Springer Berlin Heidelberg, Berlin, Heidelberg, pp. 267–294.

Furre, A.K., Eiken, O., Alnes, H., Vevatne, J.N., Kiaer, A.F., 2016. 20 years of monitoring CO2-injection at Sleipner. In: 13th International Conference on Greenhouse Gas Control Technologies (GHGT). Lausanne, SWITZERLAND. Elsevier Science Bv, pp. 3916–3926.

Harris, C., Jackson, S.J., Benham, G.P., Krevor, S., Muggeridge, A.H., 2021. The impact of heterogeneity on the capillary trapping of CO2 in the Captain Sandstone. Int. J. Greenhouse Gas Control 112, 103511.

Heidaryan, E., Hatami, T., Rahimi, M., Moghadasi, J., 2011. Viscosity of pure carbon dioxide at supercritical region: measurement and correlation approach. J. Supercrit. Fluids 56, 144–151.

Henson, V.E., Yang, U.M., 2002. BoomerAMG: a parallel algebraic multigrid solver and preconditioner. Appl. Numer. Math. 41, 155–177.

Jackson, C.A.L., Barber, G.P., Martinsen, O.J., 2008. Submarine slope morphology as a control on the development of sand-rich turbidite depositional systems: 3D seismic analysis of the Kyrre Fm (Upper Cretaceous), Maloy Slope, offshore Norway. Mar. Pet. Geol. 25, 663–680.

Jackson, M.D., Hampson, G.J., Rood, D., Geiger, S., Zhang, Z., Sousa, M.C., Amorim, R., Brazil, E.V., Samavati, F.F., Guimaraes, L.N., 2015a. Rapid Reservoir Modeling: Prototyping of Reservoir Models, Well Trajectories and Development Options Using an Intuitive, Sketch-Based Interface, SPE Reservoir Simulation Symposium. Society of Petroleum Engineers, Houston, Texas, USA, p. 17.

Jackson, M.D., Hampson, G.J., Saunders, J.H., El-Sheikh, A., Graham, G.H., Massart, B.Y. G., 2014. Surface-based reservoir modelling for flow simulation. In: Martinius, A.W., Howell, J.A., Good, T.R. (Eds.), Sediment-Body Geometry and Heterogeneity: Analogue Studies For Modelling the Subsurface. Geological Soc Publishing House, Bath, pp. 271–292.

Jackson, M.D., Percival, J.R., Mostaghiml, P., Tollit, B.S., Pavlidis, D., Pain, C.C., Gomes, J., El-Sheikh, A.H., Salinas, P., Muggeridge, A.H., Blunt, M.J., 2015b. Reservoir modeling for flow simulation by use of surfaces, adaptive unstructured meshes, and an overlapping-control-volume finite-element method. SPE Reserv. Eval. Eng. 18, 115–132.

Jackson, W.A., Hampson, G.J., Jacquemyn, C., Jackson, M.D., Petrovskyy, D., Geiger, S., Machado Silva, J.D., Judice, S., Rahman, F., Costa Sousa, M., 2022. A screening assessment of the impact of sedimentological heterogeneity on CO2 migration and stratigraphic-baffling potential: johansen and Cook formations, Northern Lights project, offshore Norway. Int. J. Greenhouse Gas Control 120, 103762.

Jacquemyn, C., Hampson, G.J., Jackson, M.D., Petrovskyy, D., Geiger, S., Machado Silva, J.D., Judice, S., Rahman, F., Sousa, M.C., 2021a. Rapid reservoir modelling: sketch-based geological modelling with fast flow diagnostics. In: Abu Dhabi International Petroleum Exhibition & Conference.

Jacquemyn, C., Pataki, M.E.H., Hampson, G.J., Jackson, M.D., Petrovskyy, D., Geiger, S., Marques, C.C., Machado Silva, J.D., Judice, S., Rahman, F., Costa Sousa, M., 2021b. Sketch-based interface and modelling of stratigraphy and structure in three dimensions. J. Geol. Soc. London jgs2020-2187.

Kitware, Inc., 2003. The VTK User's Guide. Kitware Inc., Clifton Park NY.

Lie, K.A., Møyner, O., Krogstad, S., 2015. Application of flow diagnostics and multiscale methods for reservoir management. In: SPE Reservoir Simulation Symposium. D022S002R018.

Lie, K.A., Nilsen, H.M., Andersen, O., Møyner, O., 2016. Asimulation workflow for large-scale CO_2 storage in the Norwegian North Sea. Comput. Geosci. 20, 607–622.

Linde, N., Renard, P., Mukerji, T., Caers, J., 2015. Geological realism in hydrogeological and geophysical inverse modeling: a review. Adv. Water Resour. 86, 86–101.

MacDonald, A.C., Falt, L.M., Hektoen, A.L., 1998. Stochastic modeling of incised valley geometries. AAPG Bull. 82, 1156–1172.

Mayall, M., Jones, E., Casey, M., 2006. Turbidite channel reservoirs—Key elements in facies prediction and effective development. Mar. Pet. Geol. 23, 821–841.

Møyner, O., Krogstad, S., Lie, K.A., 2015. The application of flow diagnostics for reservoir management. SEP J. 20, 306–323.

Natali, M., Klausen, T.G., Patel, D., 2014. Sketch-based modelling and visualization of geological deposition. Comput. Geosci. 67, 40–48.

Natvig, J.R., Lie, K.A., 2008. Fast computation of multiphase flow in porous media by implicit discontinuous Galerkin schemes with optimal ordering of elements. J. Comput. Phys. 227, 10108–10124.

Natvig, J.R., Lie, K.A., Eikemo, B., Berre, I., 2007. An efficient discontinuous Galerkin method for advective transport in porous media. Adv. Water Resour. 30, 2424–2438.

Nicot, J.-P., Hosseini, S.A., Solano, S.V., 2011. Are single-phase flow numerical models sufficient to estimate pressure distribution in CO2 sequestration projects? Energy Procedia 4, 3919–3926.

Noelle, S., Pankratz, N., Puppo, G., Natvig, J.R., 2006. Well-balanced finite volume schemes of arbitrary order of accuracy for shallow water flows. J. Comput. Phys. 213, 474–499.

Nordbotten, J.M., Aavatsmark, I., Eigestad, G.T., 2007. Monotonicity of control volume methods. Numer. Math. 106, 255–288.

Olsen, L., Samavati, F.F., Sousa, M.C., Jorge, J.A., 2009. Sketch-based modeling: a survey. Comput. Graph. 33, 85–103.

Onoja, M.U., Shariatipour, S.M., 2018. The impact of gradational contact at the reservoir-seal interface on geological CO2 storage capacity and security. Int. J. Greenhouse Gas Control 72, 1–13.

Osman, H., Graham, G.H., Moncorge, A., Jacquemyn, C., Jackson, M.D., 2021. Is cell-to-cell scale variability necessary in reservoir models? Math. Geosci. 53, 571–596.

Peaceman, D.W., 1983. Interpretation of well-block pressures in numerical reservoir simulation with non-square grid blocks and anisotropic permeability. Soc. Petrol. Eng J 23, 531–543.

Pereira, T., Brazil, E.V., Macêdo, I., Sousa, M.C., de Figueiredo, L.H., Velho, L., 2011. Sketch-based warping of RGBN images. Graph Model. 73, 97–110.

Pyrcz, M.J., Catuneanu, O., Deutsch, C.V., 2005. Stochastic surface-based modeling of turbidite lobes. AAPG Bull. 89, 177–191.

Rasmussen, A., Lie, K.-A., 2014. Discretization of flow diagnostics on stratigraphic and unstructured grids. In: 14th European Conference on the Mathematics of Oil Recovery 2014.

Reynolds, C.A., Blunt, M.J., Krevor, S., 2018. Multiphase flow characteristics of heterogeneous rocks from CO2 storage reservoirs in the United Kingdom. Water Resour. Res. 54, 729–745.

Scheidt, C., Caers, J., 2009. Uncertainty quantification in reservoir performance using distances and kernel methods-application to a West Africa deepwater turbidite reservoir. Spe J. 14, 680–692.

Schroeder, W.J., Ibanez, L., Martin, K.M., 2004. Software process: the key to developing robust, reusable and maintainable open-source software. In: 2004 2nd IEEE International Symposium on Biomedical Imaging: Nano to Macro (IEEE Cat No. 04EX821), pp. 648–651. Vol. 641.

Shahvali, M., Mallison, B., Wei, K., Gross, H., 2012. An alternative to streamlines for flow diagnostics on structured and unstructured grids. Spe J. 17, 768–778.

Shook, G.M., Mitchell, K.M., 2009. A robust measure of heterogeneity for ranking earth models: the F PHI curve and dynamic lorenz coefficient. In: SPE Annual Technical Conference and Exhibition. New Orleans, Louisiana. Society of Petroleum Engineers, p. 13.

Trevisan, L., Krishnamurthy, P.G., Meckel, T.A., 2017. Impact of 3D capillary heterogeneity and bedform architecture at the sub-meter scale on CO2 saturation for buoyant flow in clastic aquifers. Int. J. Greenhouse Gas Control 56, 237–249.

Watson, F., Krogstad, S., Lie, K.-A., 2021. The use of flow diagnostics to rank model ensembles. Comput. Geosci.

Zhang, Y., Bansal, N., Fujita, Y., Datta-Gupta, A., King, M.J., Sankaran, S., King, M.J., 2016. From streamlines to fast marching: rapid simulation and performance assessment of shale-gas reservoirs by use of diffusive time of flight as a spatial coordinate. SPE J. 21, 1883–1898.

Zhang, Z., Geiger, S., Rood, M., Jacquemyn, C., Jackson, M., Hampson, G., De Carvalho, F.M., Silva, C.C.M.M., Silva, J.D.M., Sousa, M.C., 2020. Fast flow computation methods on unstructured tetrahedral meshes for rapid reservoir modelling. Comput. Geosci. 24, 641–661.